MECSOL 2022 - Proceedings of the 8th International Symposium on Solid Mechanics
M.L. Bittencourt, J. Labaki, L.C.M. Vieira Jr. and E. Mesquita (Editors), Campinas SP, Brazil, October 17th to 19th, 2022

Dynamic Modeling of a Turbo-Pump Rotor Subjected to Flight Maneuvers

Sâmela Fernandes Pereira de Lima [1], Carlos d'Andrade Souto [2]

[1] Technological Institute of Aeronautics, Department of Science and Aerospace Technology, *Praça Mal. Eduardo Gomes, 50 – Vila das Acácias CEP: 1222890, São José dos Campos, SP* – Brazil.

[2] Division of Integration and Tests, Institute of Aeronautical and Space, Department of Science and Aerospace Technology, *Praça Mal. Eduardo Gomes, 50 – Vila das Acácias CEP: 1222890, São José dos Campos, SP* – Brazil.

Abstract: Liquid propellant engines are widely used in satellite launching vehicles for providing a high level of energy and the ability to control the thrust intensity. These engines require efficient propellant pumping systems. High-powered engines operate under high pressure in the combustion chamber and thus, fuel and oxidant must be injected at high enough pressures. Turbo pumps can pump propellants with the required pressure level. The rotor of a turbopump rotates at thousands of revolutions per minute and is subject to the vibrations inherent to its operation and also to the dynamic loads arising from the launch vehicle's trajectory. In this work, the effect that flight maneuvers of a satellite launching vehicle have on the transverse vibrations of a turbine pump rotor is analyzed. A rotor dynamics model with flexible shafts and hard disks was modeled and implemented in numerical computing software to perform the analysis.

Keywords: maneuver, rotor-dynamics, turbo pump, launching vehicles, liquid rocket engine.

INTRODUCTION

In a real rotor, part of the rotation energy is converted into lateral motions. Even in rotors built according to tightened geometric tolerances, there will be slight deviations from the ideal condition and consequently, vibrations are unavoidable. Moreover, turbo pump rotors usually operate at supercritical speeds (Sias et al., 2011) and the casing-rotor clearances can be pretty small (Porto, 2011). Thus, it is important to evaluate the lateral displacements of the rotor (dynamic characteristics) and its responses to the loads during its operation (Lalanne and Ferraris, 1990).

In the case of an embedded rotor in a vehicle, it is also important to consider the behavior during a maneuver, as the rotor's dynamic response will be influenced by the dynamic loading coming from the vehicle (Lin and Meng, 2003. Hou et al., 2015). Studies on the dynamics of embedded rotors including the effects of maneuvering on aircraft (Chen et al., 2020) and marine machinery were carried out (Zhansheng, 2015). The dynamic behavior of a cruise missile turbojet rotor subjected to dynamic loads caused by the operation maneuvers was analyzed by the 1st author (Lima, 2020).

In this work, the lateral dynamic response of a turbo pump rotor subjected to flight maneuvers of a launch vehicle is evaluated. The analysis was developed by a computational routine for flexible rotors dynamics with hard disks and was implemented by the authors in Matlab scientific computing software.

MATHEMATICAL MODELING

The approach used for the mathematical modeling considers the rotor shaft as flexible and the discs as hard (represented by point masses).

The analysis of the rotor-bearings system was developed through the implementation of the finite element method for rotor dynamics as described in Lalanne and Ferraris, 1990. The model of the rotor-bearing assembly consists of shaft elements (beams), disc elements (point masses), and bearing elements (stiffness and damping). The motion equations for each component of the system can be obtained by applying the Lagrange's Equation, displayed in Eq. 1, for expressions of the kinetic and potential energy.

$$\frac{d}{dt}\left(\frac{\partial T}{\partial \dot{q}}\right) - \frac{\partial T}{\partial q_i} + \frac{\partial U}{\partial q_i} = F q_i \tag{1}$$

Thus, the global motion equation describing the set rotor can be obtained from the sum of the components equations.

Shaft element

The motion equation of a shaft element is given in matrix form by Eq. 2. Detailed expressions of the matrices in Eq. 2 can be obtained in Lalanne and Ferraris, 1990. The shaft element adopted in this work uses linear interpolation, having 2 nodes and 4 degrees of freedom per node, as described in Eq. 3.

$$[M_S^e]\{\ddot{x}_S^e(t)\} - \Omega[G_S^e]\{\dot{x}_S^e(t)\} + [K_S^e]\{x_S^e(t)\} = \{f_S^e(t)\} \tag{2}$$

$$\{x_s(t)\} = \{u_1 w_1 \theta_1 \Psi_1 u_2 w_2 \theta_2 \Psi_2\} \tag{3}$$

Where $[M_i^e]$ is the mass matrix, $[G_i^e]$ the gyroscopic matrix and $[K_i^e]$ the stiffness matrix. The acceleration, velocity, displacement and force nodal vectors are respectively: $\{\ddot{x}_i^e(t)\}$, $\{\dot{x}_i^e(t)\}$, $\{x_i^e(t)\}$ and $\{f_i^e(t)\}$.

Discs

For the disc elements, the matrix motion equation is presented in Eq. 4 and the Eq. 5 shows the nodal displacement vector.

$$[M_d^e]\{\ddot{x}_d^e(t)\} - \Omega[G_d^e]\{\dot{x}_d^e(t)\} = \{f_d^e(t)\} \tag{4}$$

$$\{x_d(t)\} = \{u\ w\ \theta\ \Psi\} \tag{5}$$

Where $[M_d^e]$ is given by the summation of the system mass and inertias matrices as described in Lalanne and Ferraris, 1990.

Bearings

The equations of motion of a bearing element are given in Eq. 6. The degrees of freedom are the same given by Eq. 5.

$$[C_b^e]\{\dot{x}_b^e(t)\} + [K_b^e]\{x_b^e(t)\} = \{f_b^e(t)\} \tag{6}$$

Rotor-bearings system

Using the usual procedure for assembling global equations for the finite element method, it is possible to assemble the motion equations of the shaft, discs and bearings elements in a single global matrix equation, which describes the whole rotor-bearing system behavior. This equation is shown below, Eq. 7:

$$[M]\{\ddot{x}(t)\} + [D(\Omega)]\{\dot{x}(t)\} + [K]\{x(t)\} = \{f(t)\} \tag{7}$$

Where $[D(\Omega)]$ is given by Eq. 8 and $[C]$ represents the damping matrix.

$$[D(\Omega)] = ([C] - \Omega[G]) \tag{8}$$

ANALYSIS

Unbalance response

Considering the rotor in a real condition, the centers of mass and rotation are not coincident, and part of the rotation energy is converted into lateral motions.

To represent this effect, a concentrated unbalance mass is added to the discs. The external force generated due to the displacement of this mass is described in Eq. 9.

$$\{F\} = \{F_s\}\sin(\Omega t) + \{F_c\}\cos(\Omega t) \tag{9}$$

Where:

$$\{F_s\} = \{u_1 w_1 \theta_1 \Psi_1 \dots u_n w_n \theta_n \Psi_n\}^T = \{me\Omega^2 \sin(\Omega t)\ 0\ 0\ 0 \dots 0\ 0\ 0\ 0\}^T \tag{10}$$

$$\{F_c\} = \{u_1 w_1 \theta_1 \Psi_1 \dots u_n w_n \theta_n \Psi_n\}^T = \{0\ me\Omega^2 \cos(\Omega t)\ 0\ 0 \dots 0\ 0\ 0\ 0\}^T \tag{11}$$

And the system response to this external force is given by Eq. 12.

$$\{Q\} = \{Q_S\}sin(\Omega t) + \{Q_C\}\,cos(\,\Omega t) \tag{12}$$

By replacing Eq. 9 and Eq. 12 in the global equation of the rotor-bearing system, one obtains:

$$\begin{Bmatrix} Q_s \\ Q_c \end{Bmatrix} = \begin{bmatrix} [K] - \Omega^2[M] & -\Omega[D(\Omega)] \\ \Omega[D(\Omega)] & [K] - \Omega^2[M] \end{bmatrix}^{-1} \begin{Bmatrix} F_s \\ F_c \end{Bmatrix} \tag{13}$$

Eigenvalue analysis

In order to obtain the system natural frequencies and vibration modes, it is necessary to solve the homogeneous version of the global equation. The usual procedure is to transform the Eq. 7 into a first order matrix equation and use standard algorithms to solve the eigenvalue problem.

Therefore, Eq. 14 allows calculating the natural frequencies and eigenvectors for each value of Ω and plotting on a diagram.

$$[A]\{\dot{q}\} + [B]\{q\} = \{F\} \tag{14}$$

Where $[A]$ and $[B]$ are given in Eq. 15 and Eq. 16.

$$[A] = \begin{bmatrix} [M] & [0] \\ [0] & -[K] \end{bmatrix} \tag{15}$$

$$[B] = \begin{bmatrix} [D(\Omega)] & [K] \\ [K] & [0] \end{bmatrix} \tag{16}$$

The coordinates and the force nodal vectors are given in the Eq. 17 and Eq. 18.

$$\{q\} = \begin{Bmatrix} \dot{x}(t) \\ x(t) \end{Bmatrix} \tag{17}$$

$$\{F\} = \begin{Bmatrix} \{0\} \\ \{0\} \end{Bmatrix} \tag{18}$$

Effects of the forces from maneuvers

Due to the maneuvers the launch vehicle performs during its trajectory, the turbopump rotor is subjected to additional forces and its effect on the dynamic response can lead to excessive lateral displacements of the rotor.

The *VLS-alfa* is a launch vehicle project under development at the Brazil's Institute of Aeronautics and Space. It is composed by the first stage with four S43 solid thrusters, the second stage with one of the same kind, and the third stage consisting of a 75 KN thrust liquid propellant engine (L75 engine), (Mota, 2015).

The turbopump is placed in vertical position in L75. Its rotor operation speed is 24000 rev per minute (Sias et al., 2015). The *VLS-alfa* and the L75 engine in its third stage are displayed in Fig.1.

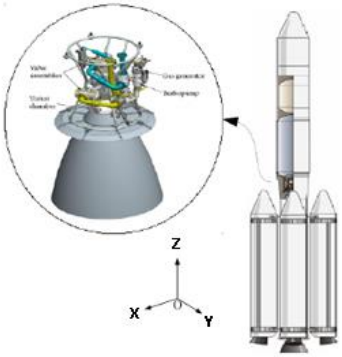

Figure 1 - L75 engine on VLS-alfa 3rd stage (adapted from (Sias et al, 2015))

A rotor, its foundation and its coordinates system used in this work is displayed in Fig. 2, extracted from (Zhandheng et al., 2015).

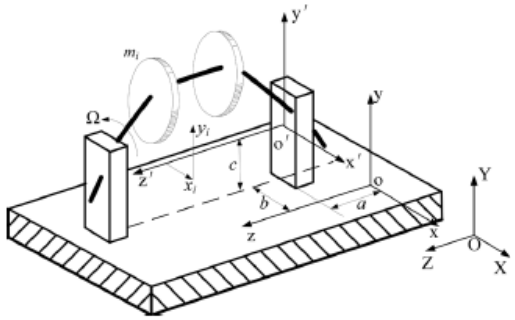

Figure 2 - Rotor, its foundation, and its coordinates systems

In Figs. 1 and 2 the launching rocket displacements are described in the inertial system fixed to the ground OXYZ and the rotor foundation motions are described in oxyz. The rotor position in relation to the foundation and its shaft lateral motions are described in the o'x'y'z' coordinate system.

Considering that the forces generated by the maneuvers act predominantly in the rotor components with greater mass, the discs, the rotor lateral motions can be described by Eq. 19 (Zhandheng et al., 2015).

$$M_i\ddot{q}_i + \left(C_i + G_i + C_{J,i}\right)\dot{q}_i + \left(K_i + K_{J,i}\right)q_i = F_{u,i}(t) + F_{g,i}(t) + F_{J,i}(t) \tag{19}$$

Where the forces are given by the equation below:

$$F_{u,i}(t) = \begin{bmatrix} m_i e_i \Omega^2 \cos\left(\Omega t + \varphi_{i,0}0\right) \\ m_i e_i \Omega^2 \sin\left(\Omega t + \varphi_{i,0}0\right) \\ 0 \\ 0 \end{bmatrix} \tag{20}$$

$$F_{g,i}(t) = \begin{Bmatrix} 0 \\ 1 \\ 0 \\ 0 \end{Bmatrix} m_i \, \mathrm{g} \cos\left(\theta_{j,x}\right) \tag{21}$$

$$F_{J,i}(t) = \begin{Bmatrix} A \\ B \\ C \\ D \end{Bmatrix} \tag{22}$$

The mass of i-th disk is m_i and the mass unbalance eccentricity is e_i and the nodal displacement vector is described by Eq. 23.

$$q_i = [x_i \;\; y_i \;\; \theta_{x,i} \;\; \theta_{y,i}] \tag{23}$$

Where x_i represents the horizontal displacements, y_i the vertical displacements of the i-th disk. The angles $\theta_{x,i}$ and $\theta_{y,i}$ represents the rotations around horizontal and vertical axes.

It was considered as a hypothesis for the trajectory of the launch vehicle that it does not suffer angular displacements around the Y and Z axes (the rocket moves in the Y-Z plane without rolling movements). This means that some simplifications can be made in the forces expressions generated by the maneuvers (Zhandheng et al., 2015):

$$X = \dot{X} = \ddot{X} = 0 \tag{24}$$

Some of the angular displacements are considered null:

$$\theta_{J,y} = \theta_{J,y} = \dot{\theta}_{J,y} = \dot{\theta}_{J,z} = \ddot{\theta}_{J,y} = \ddot{\theta}_{J,z} = 0 \tag{25}$$

Where the index *J* indicates the foundation (launch vehicle) motion in relation to the inertial system fixed to the ground.

The angular speed of the maneuver is:

$$\omega_m = \dot{\theta}_{J,x} \tag{26}$$

Further, the right-hand side terms of Eq. 22 are given by the equations bellow:

$$A = 0 \tag{27}$$

$$B = -m_i\left(\ddot{y}_j - \omega_m \dot{z}_j\right) + m_i c\omega_m^2 + m_i e_i \omega_m^2 sin(\Omega t) - m_i g \cos(\omega_m t) \quad (28)$$

$$D = 0 \quad (29)$$

$$E = I_p\, \Omega\, \omega_m \quad (30)$$

The component $\ddot{y}_j$ is the rocket acceleration on the Y axis, $\dot{z}_j$ is the rocket speed on the Z axis, m_i is the disk mass, e_i represents the unbalance and Ω is the rotation speed of the rotor.

SYSTEM ANALYZED

The case studied in this work is the turbo pump used in the L75 engine which can be seen in Fig. 3. The engine is presented in (Almeida and Pagliuco, 2014) and shown in Fig. 3.

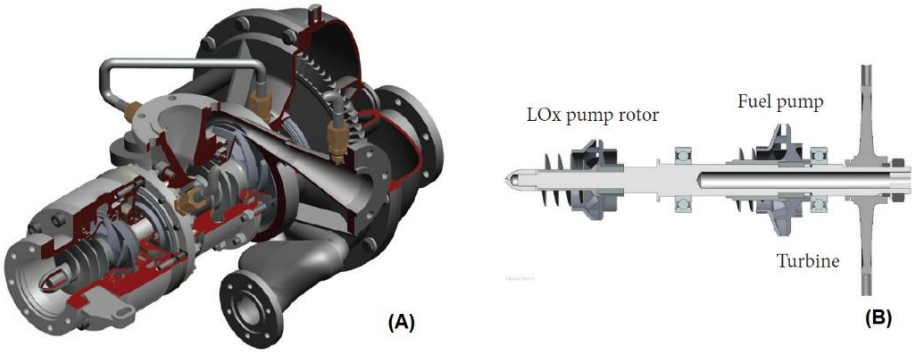

Figure 3 - A: Turbopump, B: Rotor assembly

In Fig. 4 it is possible to observe the shaft shape and the positions of the rotor components.

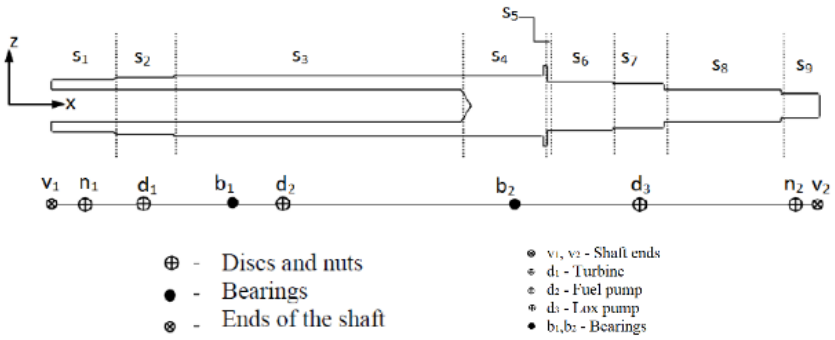

Figure 4 - Rotor-dynamic model

The position of the different rotor components is shown in Tab. 1, the bearings properties of stiffness and damping are given in Tab. 2 (Sias et al., 2015), the properties of mass and inertia are given in Tab. 3 and the unbalance masses are shown in Tab. 4 (determined by considering G2.5 quality grade in ISO 21940-11:2016 Standard). As most of liquid rocket engine turbo-pumps, the L75 turbopump uses contact ball bearings (Zhang and Tian, 2018). The coupling between the vertical and horizontal directions in the stiffness and damping of the bearings was considered null (Sias et al., 2015).

Table 1 - Position of the Components

Elements	x [m]
v_1	0
b_1	0.095
b_2	0.225
d_1 (Turbine)	L
d_2 (Fuel Pump)	2.7411L
d_3 (Lox Pump)	6.7337L

Table 2 - Bearings Properties

Bearings	K_{yy} [N/m]	K_{zz} [N/m]	C_{yy} [Ns/m]	C_{zz} [Ns/m]
b_1, b_2	25.48×10^6	25.48×10^6	0.5×10^3	0.5×10^3

Table 3 - Disks Properties

Elements	d_1	d_2	d_3
Mass [kg]	2.379	0.17344	0.12466
Jx [kg.m^2]	1.082×10^{-2}	1.889×10^{-4}	9.1375×10^{-5}
Jy [kg.m^2]	5.454×10^{-3}	1.0095×10^{-4}	5.0715×10^{-5}
Jz [kg.m^2]	5.454×10^{-3}	1.0045×10^{-4}	5.0433×10^{-4}

Table 4 - Unbalance Masses

Disk	Turbine	Fuel Pump	Lox Pump
Unbalance [g.mm]	20.8025	13.7587	7.9810

RESULTS

The rotor studied here was analyzed in (Lima and Souto, 2020) and its first two critical speeds determined: 19121 rpm and 34193 rpm. The corresponding 1st and 2nd forward modes frequencies are 318.68 Hz and 569.88 Hz. Its Campbell's diagram is displayed in Fig. 5.

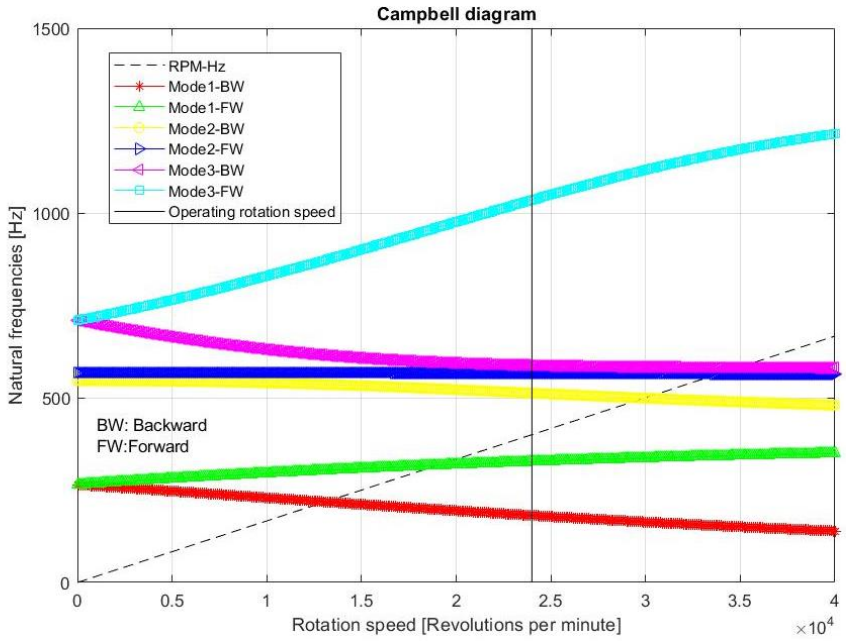

Figure 5 – Turbopump Campbell diagram

In this work two situations were analyzed: the rotor on the ground (fixed foundation) and the rotor subjected to dynamic loads originating from the launcher's trajectory shown in Fig.6. The curve described by the trajectory belongs to the vertical plane.

The Eq. 19 was solved using the Newmark-HHT numerical integration method (Chen et al., 2020). All results were obtained for a fixed turbo pump rotation speed of 24000 rev per minute.

Rotor on a fixed foundation on the ground

In this condition the unbalance forces on the disks are considered the only forces acting on the rotor. The lateral displacement of the Lox pump impeller center is displayed in Fig. 6. Due to the bearings' isotropy, the displacement in both lateral directions (x and y directions in the o'x'y'z 'coordinate system shown in Fig.2.) is the same.

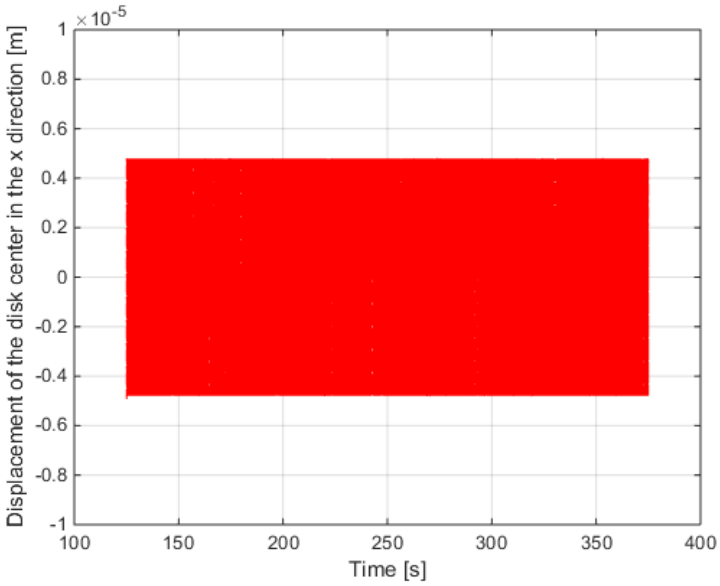

Figure 6 – Lateral (x and y) displacement of the Lox pump impeller center

Launcher vehicle trajectory

In this situation the rocket performs a flight with maneuvers and all movements are contained in the vertical plane (y-Z in Fig.1).

The flight event sequence considered in this work was adapted from the results of (Mota, 2015) and is composed of the following steps: 1) At lift-off, the 1st stage (composed of the four “boosters”) engines are ignited; 2) Ignition of the 2nd stage; 3) End of the burning of the 1st stage “boosters” and their disposal; 4) End of the burning of the 2nd stage and its disposal. Ignition of the 3rd stage (L75 engine); 5) Discard of the fairing; 6) Interruption of the 3rd stage motor operation. Start of the non-propelled phase of the flight. The non-propelled flight is represented by the part where there is a small decrease in the speed of the VLS-alpha (can be observed in Fig. 7); 7) End of non-propelled flight, re-ignition of 3rd stage engine; 8) End of the 3rd stage engine burn and its disposal. Insertion of the satellite in orbit. We analyzed the maneuvers effect on the turbopump rotor in the 1st phase of the 3rd stage propelled flight (step 4).

In Fig. 8 the launching vehicle vertical displacement as a function of the horizontal displacement is displayed. The analyzed part of the flight is highlighted in red on the curve.

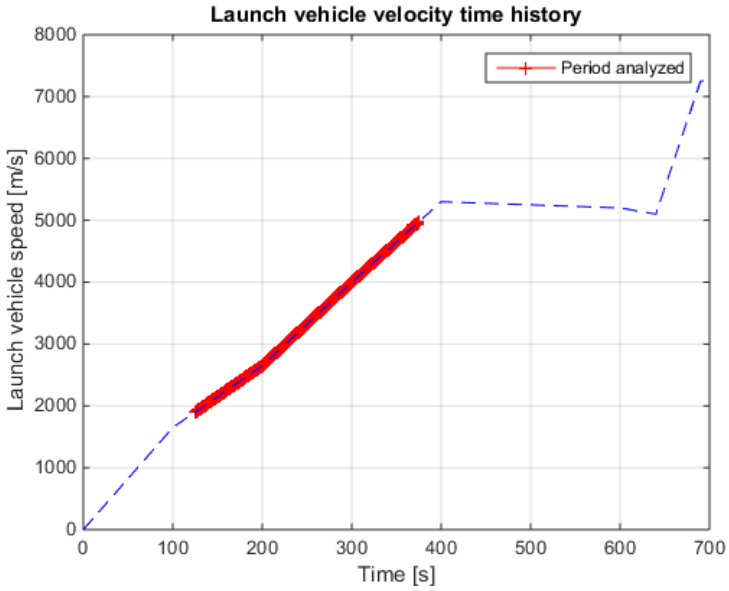

Figure 7 – *Launch vehicle velocity profile*

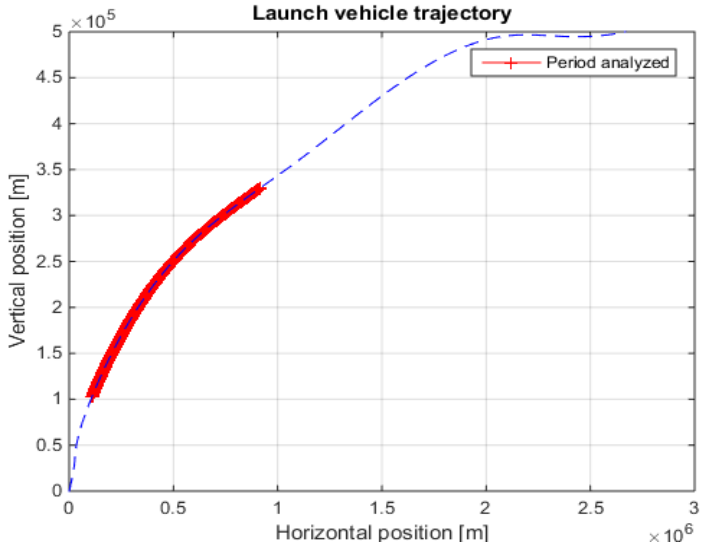

Figure 8 – Launch vehicle trajectory

In this situation, the lateral displacement of the Lox pump impeller center has a behavior described by Fig. 9 (x displacements) and Fig. 10 (y displacements).

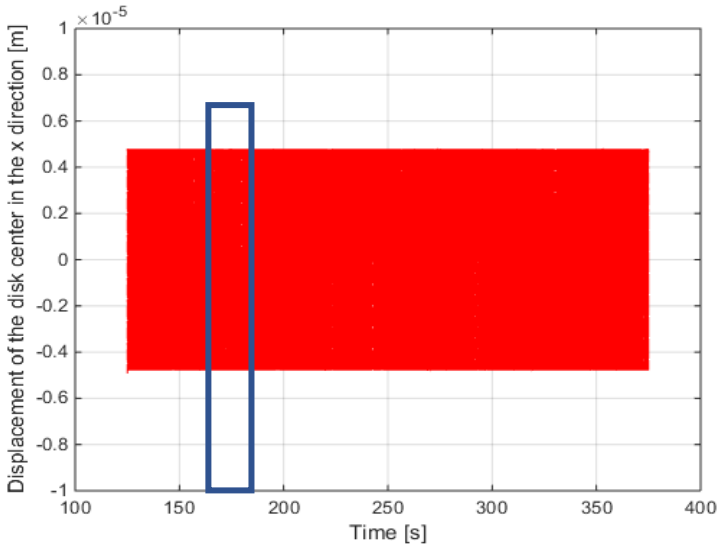

Figure 9 – Lateral displacement of the Lox pump impeller center (x direction)

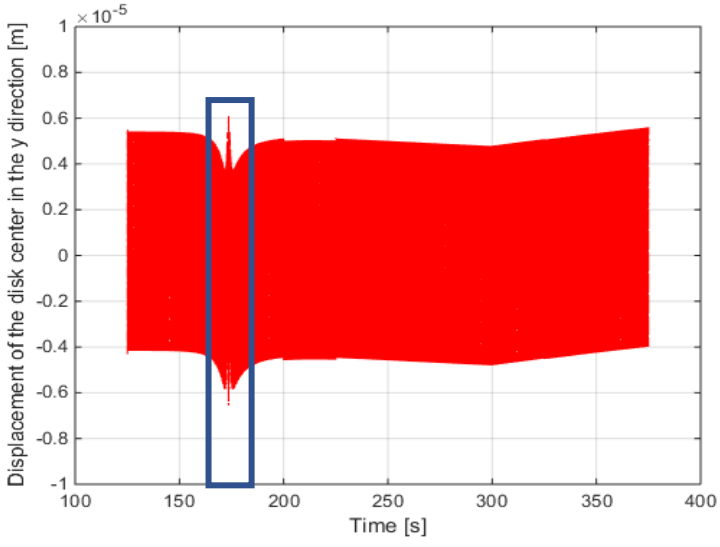

Figure 10 – Lateral displacement of the Lox pump impeller center (y direction)

It can be noticed that the rotor behavior is influenced by the maneuvers only in the y direction. At the period analyzed (125 to 375 seconds) while in the y direction the center of the disk oscillates irregularly around an equilibrium position that does not coincide with the imaginary line that joins the centers of the bearings (axis o'-z 'in Fig.2), in the x-direction, the motion is sinusoidal around the original equilibrium position.

The lateral displacements of the center of the Lox pump disc for the rotor not subjected to maneuvers and the rotor under the effect of the maneuvers can be seen in its respective orbits, shown in Fig. 11. The time considered for the calculation of the orbits is highlighted rectangles in Figs. 9 and 10. It can be seen that the effect of the maneuvers was to move the central position of the orbit down about $1x10^{-6}$ m in the y direction (10.5% of the orbit diameter), without changing its shape.

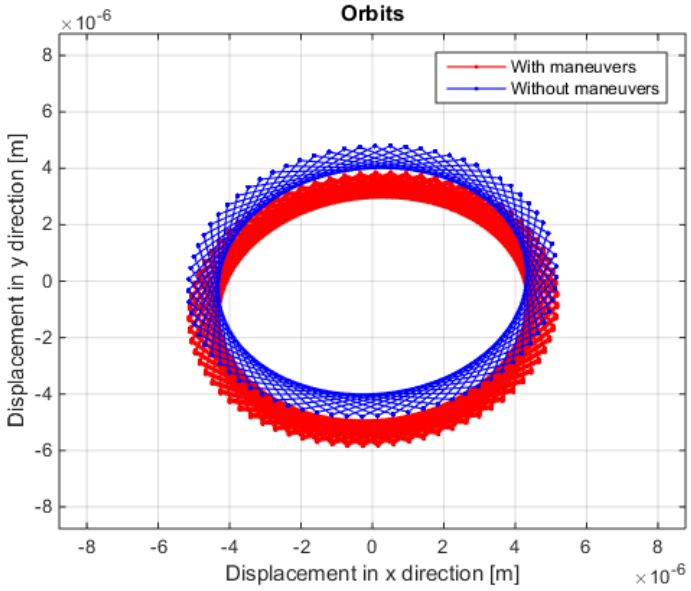

Figure 11 – Orbit plots for rotor with and without maneuver effect (Lateral displacements of the Lox pump impeller center)

CONCLUSION

A computational routine for dynamic analysis of flexible rotors with hard disks developed by the authors was used to analyze the lateral vibrations of a turbo pump rotor during the maneuvers of a launch vehicle. The vehicle's trajectory was considered contained in the vertical plane. It was possible to verify that the maneuvers affect the lateral displacement of the rotor in the direction contained in the plane where the launcher travels, but do not alter the shape of the orbits described by the centers of the rotor discs.

The combined analysis of the vehicle trajectory and rotor lateral dynamics allowed us to describe the behavior of the rotor in a real operating situation. The presented methodology can be extended to more complex trajectories and applied to embedded rotors in other types of vehicles.

ACKNOWLEDGEMENT

This study was financed in part by the *Coordenação de Aperfeiçoamento de Pessoal de Nível Superior – Brasil* (CAPES) – Finance Code 001.

REFERENCES

Almeida, D.S., Pagliuco, C.M.M., 2014, "*Development status of L75: a Brazilian liquid propellant rocket engine*", Journal of Aeroespace Technology and Management, 6, 475-484.

Chen, X., Gan, X., Ren, G, 2020, *"Effect of flight/structural parameters and operating conditions on dynamic behavior of a squeeze-film damped rotor system during diving-climbing maneuver",* Proceedings of Institution of Mechanical Engineers, Part G: Journal of Aerospace Engineering (0)-(0) 1-31.

Hou, L., Chen, Y., Cao, Q., Zhang, Z, 2015, *"Turning maneuver caused response in an aircraft rotor-ball bearing system"*, Journal Nonlinear Dynamics and Chaos in Engineering Systems, v. 79, n. 1, pp. 229 – 240.

ISO 21940-11:2016 *Standard Mechanical vibration — Rotor balancing — Part 11: Procedures and tolerances for rotors with rigid behavior.*

Lalanne, M., Ferraris, G., 1990, "*Rotordynamics prediction in engineering",* Lyon: Wiley.

Lima, S.F.P., 2020, *"Dynamic modeling of a cruise missile turbo-reactor rotor"*, University of Taubaté, Taubaté, Brazil, in Portuguese.

Lima, S.F.P., Souto, C.A., 2020, "*Dynamic modeling of a liquid rocket engine turbo pump rotor*", CILAMCE 2020 Proceedings of the XLI Ibero-Latin-American Congress on Computational Methods in Engineering, ABMEC Foz do Iguaçu/PR, Brazil, November 16-19.

Lin, F., Meng, G., 2003, *"Study on the dynamics of a rotor in a maneuvering aircraft"*, Shanghai: Journal of Vibration and Acoustics, v. 125, pp 324 – 327.

Mota, F.A.S., 2015, "*Modeling and simulation of launch vehicles using object-oriented programming*", Doctorate Thesis of the Graduate Course in Space Engineering and Technology, São José dos Campos, SP, Brazil.

Porto, B.F., 2011, "*Design of the rotor assembly of a turbine pump for a liquid propulsion rocket engine*", Professional Master's Diss. in Aerospace Engineering-Instituto Tecnológico de Aeronáutica, S. J. dos Campos, Brazil, 99pp.

Sias, D.F., Barros, E., Souto, C.A., Almeida, D.S., 2015, "*Dynamic Analysis of a Liquid Rocket Turbopump Unit*", *23rd ABCM International Congress of Mechanical Engineering* December 6-11, Rio de Janeiro, RJ, Brazil

Zhang, X., Tian, A., 2018 *IOP Conf. Ser.: Mater. Sci. Eng.* **394** 032138.

Zhansheng, L., Guanghui, Z., Ruixian, M., Shupeng, L., 2015, *"Nonlinear dynamic characteristics of journal bearing-rotor system considering the pitching an rolling motion for marine machinery"***,** Harbin: Journal of Engineering for the Maritime Environment, Vol. 229 (1) 95-107.

Zink, E., Bourdon, D., Almeida, D.S., Pagliuco, C. M., Kitsche, W., Wagner, B., Langel, G., 2017, "*Biofuel Turbopump Development Strategy: L75 Liquid Oxygen and Ethanol Engine Case", 53rd AIAA/SAE/ASEE Joint Propulsion Conference*.

RESPONSIBILITY NOTICE

The authors are the only parties responsible for the printed material included in this paper.